

MODELS OF PLUMES: THEIR FLOW, THEIR GEOMETRIC SPREADING, AND THEIR MIXING WITH INTERPLUME FLOW

S. T. Suess

NASA Marshall Space Flight Center/ES82, Huntsville, AL 35812, USA

ABSTRACT

There are two types of plume flow models: (i) 1D models using ad hoc spreading functions, $f(r)$. (ii) MHD models. 1D models can be multifluid, time dependent, and incorporate very general descriptions of the energetics. They confirm empirical results that plume flow is slow relative to requirements for high speed wind. But, no published 1D model incorporates the rapid local spreading at the base ($f_i(r)$) which has an important effect on mass flux. The one published MHD model is isothermal, but confirms that if $\beta \ll 1$ then the field is nearly potential below $\sim 50,000$ km. Building on the MHD result, we apply a two scale approximation to calculate $f_i(r)$. We also compute the global spreading ($f_g(r)$) out to $5.0 R_{\text{SUN}}$ imposed by coronal hole geometry. Global MHD models provide a potent method of calculating $f_g(r)$.

Unambiguous plume signatures have not yet been found in the solar wind. This is probably due to strong mixing of plume and interplume flows near the Sun. We describe a physical source for strong mixing due to the observed flows being unstable to shear instabilities that lead to rapid disruption.

Key words: Plumes, Theory, MHD, Kelvin-Helmholtz

1. INTRODUCTION

Plumes are bright quasi-radial rays between one and several R_{SUN} in coronal holes. They are observed during eclipses and, e.g., from SOHO and SPARTAN-201. Using SOHO, DeForest et al. (1998) have finally unambiguously shown all plumes lie over photospheric magnetic flux concentrations, although not all flux concentrations have plumes. Modeling, SOHO/UVCS, and SPARTAN-201 have shown that plume flow speeds are probably $\sim 100\text{--}300$ km/s at $2.0\text{--}5.0 R_{\text{SUN}}$ (Wang, 1994; Habbal et al., 1995; Corti et al., 1997; Poletto et al., 1997) while *Interplanetary Scintillations* (IPS) show that the interplume flow speed may already be 750 km/s at $5.5 R_{\text{SUN}}$ (Grall et al., 1996). Therefore, plumes flow much more slowly than interplume plasma inside $10 R_{\text{SUN}}$.

Being bright in white light, plumes are denser than interplume plasma. This, together with the information

given above, suggests that plumes should be observable in the interplanetary medium. However, concerted searches of the Ulysses data (McComas et al., 1995; Neugebauer et al., 1995) have yielded inconclusive results. In fact, the high speed solar wind coming from coronal holes is remarkably smooth (Phillips et al., 1995). Therefore, plume and interplume plasma are mixed somewhere close to the Sun.

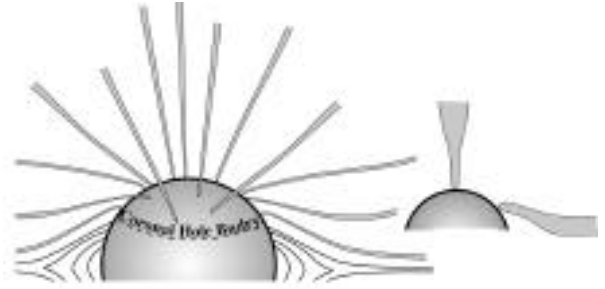


Figure 1. Plumes lie over some, not all, photospheric magnetic flux concentrations. Spreading is therefore rapid near the base and governed by the coronal hole geometry above $\sim 50,000$ km (see exaggerated plume geometry at right).

Modeling plumes therefore reduces to at least three individual problems: the flow, the geometric spreading, and the plume/interplume mixing. The flow modeling is fundamentally straightforward and has a good foundation. The directions in which it should go are clear. It is easy to model the field, or streamline, geometry of plumes because $\beta \ll 1$ in coronal holes, out to at least $10 R_{\text{SUN}}$ and possibly to 0.5 AU. Given the streamline geometry, one-dimensional (1D) solar wind models can be used to determine the flow properties in plumes using spreading functions. However, the plume/interplume mixing problem must be resolved. Plumes can be observed with LASCO to at least $10 R_{\text{SUN}}$, but are difficult to detect at 0.3 AU according to Helios 1/2 observations.

In this brief summary, flow models are reviewed first, then the technique for calculating the streamline or field geometry is discussed - since parts of it are quite new, and finally an idea is outlined for plume/interplume mixing in coronal holes to produce what is observed farther from the Sun.

2. PLUME FLOW MODELS

For the purpose of calculating plume flow in the corona, inside $\sim 10 R_{\text{SUN}}$, an acceptable assumption is that the flow is radial and that the plume geometry is expressed in terms of the “spreading function” introduced by Kopp and Holzer (1977). Section 3 will address calculating the spreading function. With these assumptions, the flow calculation reduces to a 1D problem. Specifically, this leaves only the momentum, continuity, and energy equations along the streamline, with multiple momentum and/or energy equations for multicomponent flow, plus the equation(s) of state.

In spherical coordinates, where A_o is the area at the base of a streamline or flux tube, at radius r_o , $f(r)$ is defined in terms of $A(r)$ by

$$A(r) = (r/r_o)^2 f(r) A_o \quad (1)$$

Many methods are used to solve the 1D, possibly time dependent solar wind equations. A particularly good method is as an “initial-boundary value problem” in which an essentially arbitrary initial state is allowed to relax in time until the solution is steady. This correctly deals with the critical point(s), a recovered solution is guaranteed to be stable, and it can be very efficient, numerically, if implicit numerical time differencing is used. A time dependent solution has the added benefit that it can also be used for simulations of transients. Various realizations of this approach are in the literature. Two fully implicit, noniterative models are those by Suess (1982a) and Hu et al. (1997). The later paper poses a fairly complex problem of anisotropic temperatures, heat and momentum sources, Alfvén waves, an electron-proton fluid, and inhibition of radial thermal conduction by the Archimedian spiral of the interplanetary magnetic field. The calculation was only applied to fast wind analysis, but could equally well have been applied to plumes. The differences between interplume and plume flow lie in the densities chosen, the heating terms, and in the geometry near the base of the flow.

A particular model is that by Habbal et al. (1995), discussing “less dense” and “denser” structures in coronal holes and which seems to apply to plumes. It is strongly constrained by SPARTAN 201-01 observations made of the northern polar coronal hole in April 1993. The model is two fluid (electrons and protons) and has Alfvén waves and radiative losses (Rosner et al., 1978). Radial flow is invoked in the plumes, while the spreading function is greater than unity in the interplume flow. The results are that flow speeds in plumes are less than in interplume flow. The smaller spreading function in the plumes helped produce the required enhanced density and was partly responsible for the smaller flow speed. Plots for their flow speeds in the interplume and plume are shown in Figure 2.

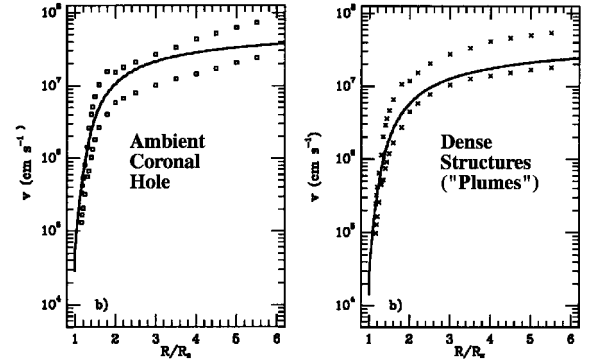


Figure 2. Flow speeds from Habbal et al. (1995): \square 's and \times 's are empirical values based on observed density, assumed spreading function, and a mass flux at 1 AU of 1.6 or $3 \times 10^8 \text{ cm}^{-3}$. The solid lines are the model computations. Left: ambient coronal hole. Right: dense structures (“plumes”).

Another particular model is that by Wang (1994), who solved the steady state equations, also produced low speed, dense plumes, but differed in the details of the physics from that of Habbal et al. Wang’s one fluid model used equal spreading functions in the plume and interplume. He constrained his model to give realistic velocities, temperatures, and mass fluxes at 1 AU, had heating and radiative losses in the corona and transition region, and used extra heating in plumes to produce their enhanced densities.

Wang’s and Habbal et al.’s models are examples of how 1D solar wind solutions can be applied equally well to plumes and the standard solar wind. Both models produce speeds similar to empirical results (Corti et al., 1997; Poletto et al., 1997) at $\sim 2 R_{\text{SUN}}$ and have densities higher than interplume plasma. However, from this point they diverge. Habbal et al. use plume/interplume spreading differences to help produce enhanced the plume density while Wang uses enhanced basal heating to do the same. Neither model invokes the rapid geometric spreading now known to exist at the base of plumes (DeForest et al., 1998) and which has been shown to be dynamically important (Del Zanna et al., 1997). Finally, the interplume flow speed is less than the reported 750 km/s at $5.5 R_{\text{SUN}}$ from IPS observations (Grall et al., 1996).

3. PLUME GEOMETRY MODELS

The geometric spreading of plumes can be computed with acceptable accuracy independently of the flow because $\ll 1$ in plumes and throughout the surrounding coronal holes from the base of the corona to at least $10 R_{\text{SUN}}$. This has been explicitly proven by Del Zanna et al. (1997), and was invoked in earlier potential field models of Newkirk and Harvey (1968) and Suess (1982b). Del Zanna et al. used an isothermal model to show that the flow has negligible effect on geometric spreading. Their results are summarized in

Figures 3 and 4. This estimate is for a simple model, but Suess and Smith (1996) have estimated for general conditions in coronal holes and found it to always be small. This is supported by *in situ* measurements on Ulysses which show that β is of O[1] at 1 AU, decreasing towards the Sun (Suess et al., 1996).

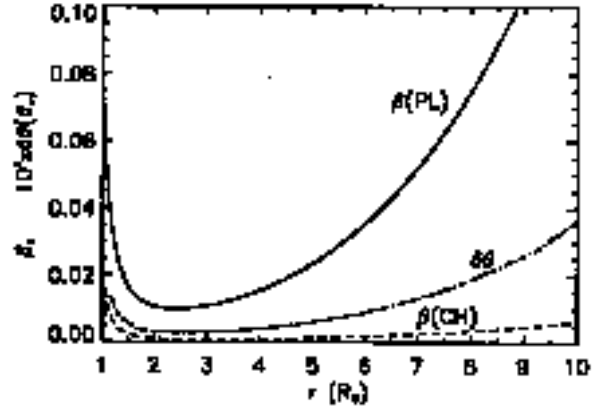


Figure 3. β on the plume axis (PL) and in the coronal hole (CH) in the Del Zanna et al. (1997) model. $\delta\theta$ is the field line displacement, at the plume half-width, away from a potential field (radians).

Given that $\beta \ll 1$, the field near the base is dominated by the magnetic flux concentrations, as shown in Figure 4, and whether a plume lies above the concentration has little influence on the geometry.

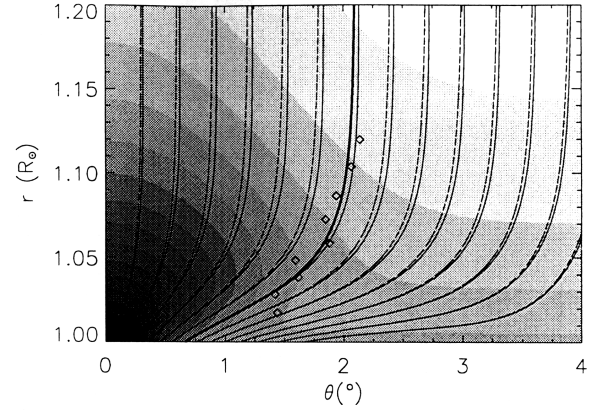


Figure 4. The plume geometry from Del Zanna et al. (1997). The corrected (solid) and unperturbed (dashed) fields are shown, along with a grey-scale plot of the density. The diamonds are plume sizes reported by Ahmad & Withbroe (1977).

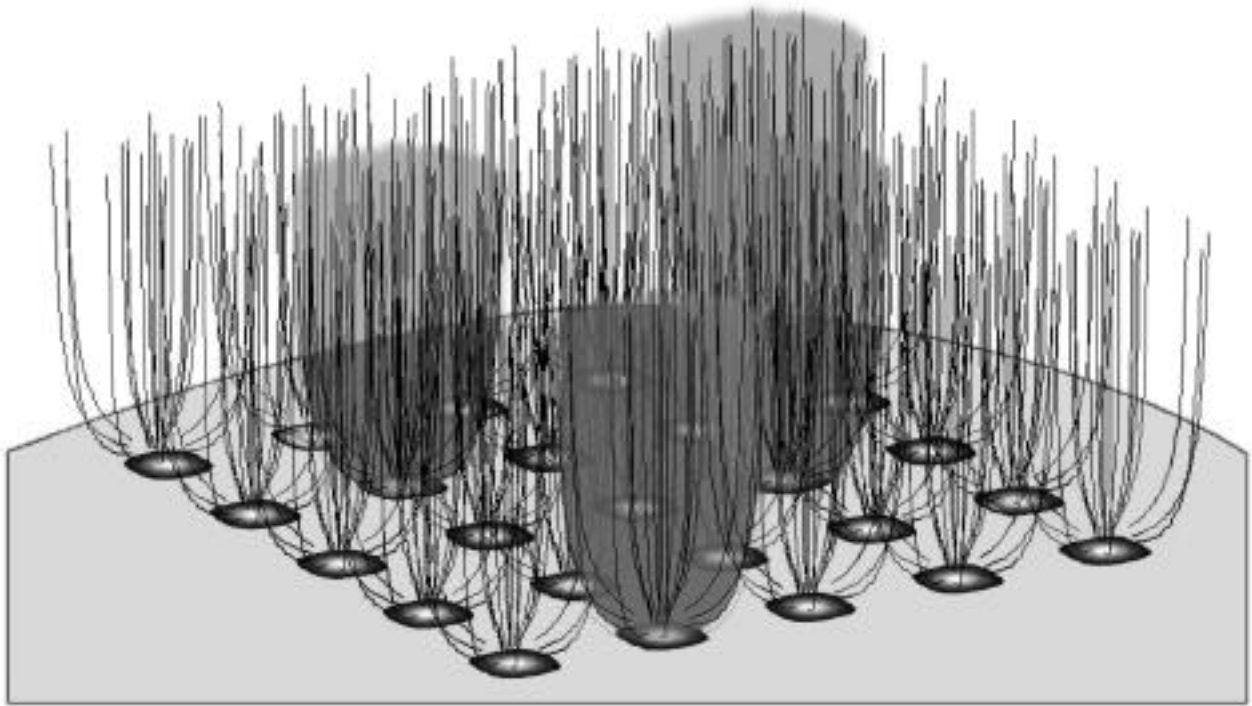


Figure 5. Array of flux concentrations at the photosphere, with rapidly spreading field lines above the photosphere to a height \sim the typical flux concentration separation distance. Some concentrations have plumes, but not all. Above $\sim 50,000$ km, the field is locally smooth in the transverse direction.

By a height comparable to the typical separation between flux concentrations, the field is smooth and is dominated by the large scale geometry of the coronal hole. This may seem counterintuitive, so a brief explanation is given. Coronal holes are open, releasing solar wind, because of the radial pressure gradient. The field is too weak to contain the plasma, but the plasma

remains small until at least $10 R_{\text{SUN}}$ because of the low density in coronal holes. This means that transverse (to the radial direction) gradients in the field will be rapidly smoothed but that transverse gradients in the plasma density have little effect on the geometry (Suess & Smith, 1996; Suess et al, 1998a). This is the reason Ulysses measured essentially constant radial magnetic field strength across the polar coronal holes and it is why plumes and adjacent interplume streamlines have the same geometric spreading above the rapid basal plume spreading region. This permits a very simple separation to be made to compute the spreading function - a *two scale approximation*. Let

$$f(r) = f_{\text{local}}(r)f_{\text{global}}(r) \equiv f_i(r)f_g(r) \quad (2)$$

Then

$$B(r) = B_o(R_{\text{SUN}}/r)^2 1/(f_i(r)f_g(r)) \quad (3)$$

With the two scale approximation, $f_i(r)$ is computed from a potential field model incorporating the distribution of magnetic flux concentrations at the photosphere, and $f_g(r)$ is computed from a global model of the corona such as that illustrated in Figure 6 (Wang et al., 1998). The calculation is described in detail by Suess et al. (1998a).

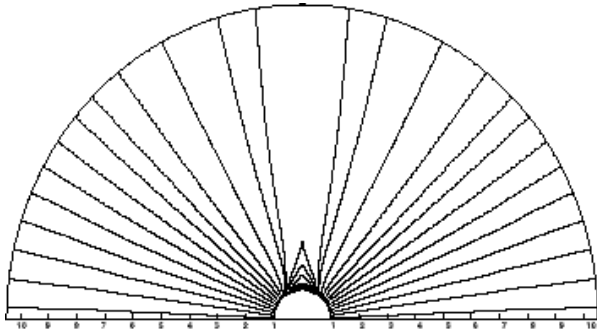


Figure 6, The magnetic field lines in the MHD global coronal model of Wang et al. (1998).

Figure 5 shows a plot of the array of flux concentrations at the base of the corona - some with plumes. The results shown below are for this rectangular distribution. A hexagonal distribution might be more appropriate for the Sun but the quantitative difference, in terms of the spreading function, is negligible (Suess et al., 1998a). A calculation with a 5% background flux, full width at half-maximum of the concentration of about 0.13 of

the distance between concentrations, results in the $f_i(r)$ shown in Figure 7. $f_i(r)$ increases rapidly from unity to ~ 13 between the photosphere and $<50,000$ km. This calculation was scaled such that the concentrations were separated by $\sim 30,000$ km. Above $50,000$ km $f_i(r)$ is constant. This is a requirement of the two-scale approximation, and is well satisfied.

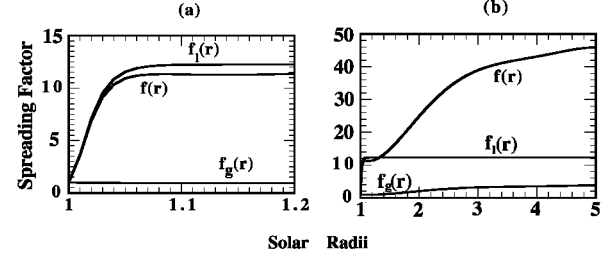


Figure 7. Combined local and global spreading factors for a flux concentration of half-width-0.13 times the concentration separation distance and a 5% background field. The global spreading is computed along the symmetry axis in the Wang et al. (1998) model (from Suess et al., 1998a).

For $f_g(r)$, the geometry is determined by the coronal hole geometry. This can either be estimated empirically, by examining coronal hole boundaries (Munro & Jackson, 1977) or theoretically, from global MHD models. MHD models show that the spreading depends only weakly on position across a hole, except very near the edges, so that empirical estimates have considerable validity. However, here we will show results from the MHD calculation of Wang et al. (1998). The Wang et al. model incorporates volumetric source terms and latitude dependent boundary conditions to obtain physically realistic flow speeds and densities in the coronal holes and reasonable temperatures and densities in the streamers. It gives a plasma throughout the coronal hole of the same magnitude as estimated by Suess and Smith (1996) and Del Zanna et al. (1997). The field lines are shown in Figure 6 for this model. We have computed $f_g(r)$ from the model for field lines near the edge and at the center of the hole. The spreading functions derived from this model are qualitatively similar to those derived from Steinolfson et al.'s (1982) model and from Suess et al.'s (1996) model, as well as those derived empirically. $f_g(r)$ along the axial field line in the model shown in Figure 6 is that plotted in Figure 7. It is seen to vary only slowly between 1.0 and 1.2 R_{SUN} , and to vary much more rapidly than $f_i(r)$ above 1.2 R_{SUN} . This is the second requirement for the applicability of the two scale approximation, and it is also well satisfied. The product of $f_i(r)$ and $f_g(r)$ gives the total spreading function, which is also plotted in Figure 7. Because of the rapid basal spreading, the total spreading ultimately reaches almost 50 at 5 R_{SUN} . The background field is very important in this model, with the *local* spreading reaching 50 for zero background.

4. MIXING OF PLUME & INTERPLUME FLOWS

Plume and interplume flow speeds are inferred to differ by at least 200 km/s at 5 R_{SUN} from empirical evidence (Grall et al., 1996; Corti et al., 1997; Poletto et al., 1998) and from models (Habbal et al., 1995; Wang, 1994). The models also suggest that the temperatures and densities could differ at 1 AU. These signatures would easily be found in Ulysses measurements of polar coronal hole flow. The rotational (corotating interaction region) interactions which otherwise obliterate plume signatures in equatorial flow are almost entirely absent at high latitude (Neugebauer et al., 1995). Yet, no obvious plume signatures have been detected. This simple empirical fact leads to the conclusion that there is mixing of plume and interplume plasmas somewhere between 10 R_{SUN} and 0.3 AU (the perihelion of Helios 1/2).

There are probably numerous processes which could lead to plume/interplume mixing. It is also possible that momentum and energy deposition in the outer corona could erase plume/interplume differences. Nevertheless, whatever other processes exist, it is easy to show that plumes will be subject to MHD Kelvin-Helmholtz (KH) shear instabilities beginning at $\sim 10 R_{\text{SUN}}$, and that these instabilities will otherwise lead to disruption of the plumes and mixing with interplume plasma. It is furthermore of interest that, because this occurs in a low to moderate plasma, the KH instability will produce Alfvénic fluctuations - potentially a source for some of the Alfvénic fluctuations observed in the solar wind. This is a strong hypothesis, based on linear stability and growth rate analysis and on extensive numerical simulations. However, no published simulations or detailed evaluations explicitly address parameters appropriate for coronal plumes so considerable analysis remains to be done with respect to this hypothesis. The physical process and existing numerical results are outlined here.

Briefly, the ordinary KH instability occurs when the shear speed between two fluids becomes too large. It is reviewed by Chandrasekhar (1961), and can occur even in an incompressible, inviscid fluid in which there is horizontal streaming. In the viscous fluid case, the interface is unstable for all wave numbers greater than a specific value determined by the velocity difference, no matter how small the velocity difference. For compressible fluids, this narrows to the shear having to be larger than the sound speed for the KH instability to occur.

Just as one might intuitively expect, the MHD KH instability occurs for shears greater than the Alfvén speed (Hardee et al., 1992; Hardee, 1995; Hardee & Clarke, 1995). This has been examined in detail for

linear stability in slab jets and in numerical simulations for slab jets and jets in cylindrical, expanding atmospheres. It has been found that the instability grows most rapidly for Alfvénic (transverse, or sinusoidal) fluctuations and that nonlinearities do not stabilize the instabilities. “The MHD KH results suggest that a jet which is initially subAlfvénic and stable to disruption will be doomed to disruption at the Alfvén point if it becomes superAlfvénic as a result of jet expansion” (Hardee et al, 1992).

Turning to coronal holes and plumes, the first thing to consider is whether the stability criterion of the MHD KH instability has any relevance. Figure 8 (Krogulec et al., 1994) shows one example of estimating the Alfvén speed in coronal holes. In the right panel, it is seen that the Alfvén speed peaks above 1000 km/s and is generally above several hundred km/s out to 10 R_{SUN} . Then, for typical field strengths, the Alfvén speed drops below ~ 400 km/s, which is typical of the expected shear between plume and interplume plasma. By way of confirmation, the Alfvén speed shown here is similar to that estimated independently by Suess (1988).

Using Figure 8 and the above discussion of the values of v in coronal holes, it is possible to construct the cartoon in Figure 9 illustrating the parameter regimes which plumes typically pass through. For moderate shear ($> \sim 300$ km/s) plumes first become superAlfvénic and then move into a high plasma regime. For small shears, it is possible that plumes would move into the high β regime before becoming shear unstable and, hence, the resulting KH instability will be more like the OHD KH instability.

The remaining important parameters governing the behavior of the KH instability are the internal and external: magnetosonic Mach numbers, Alfvén Mach numbers, and densities.

Several MHD simulations have been performed by Hardee and his colleagues. However, these have all been directed towards the analysis of astrophysical jets. Although they confirm the linear stability analysis, they do not incorporate parameters appropriate for plumes. In particular, none of the reported simulations have a magnetic field outside the jet. Nevertheless, it is instructive to examine the results shown in Figure 10 from one of the simulations. The simulation is for a slab jet in a cylindrical geometry, with an expanding atmosphere. The geometry is independent of the coordinate normal to the plane of the figure. Due to the expanding atmosphere, the shear, which is initially subAlfvénic, eventually becomes superAlfvénic. At this point, the MHD KH instability occurs and sinusoidal oscillations set in. The plot shows the resulting magnetic field lines.

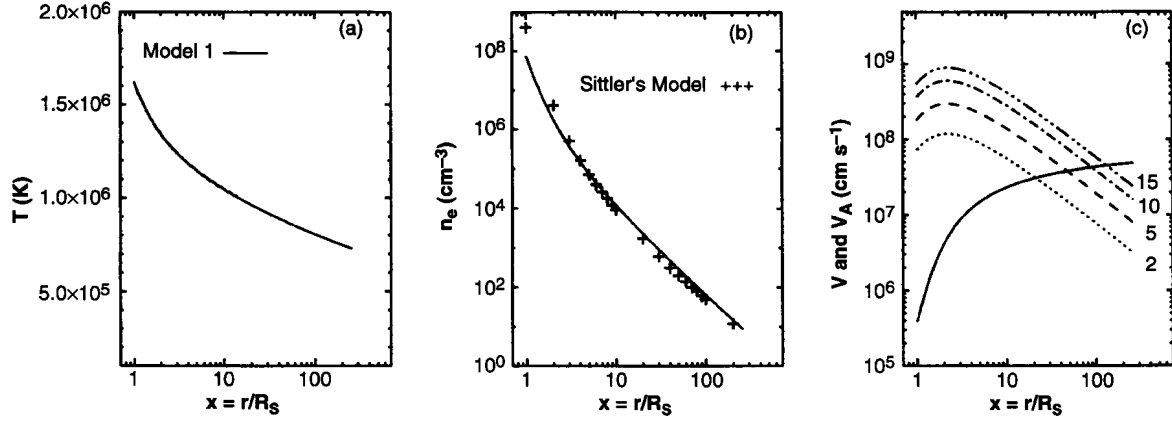


Figure 8. Temperature distribution (a), electron density (b), and flow and Alfvén speeds (c) for a model coronal hole atmosphere (Krogulec et al., 1994). The Alfvén speed has been computed for several different photospheric magnetic field strengths.

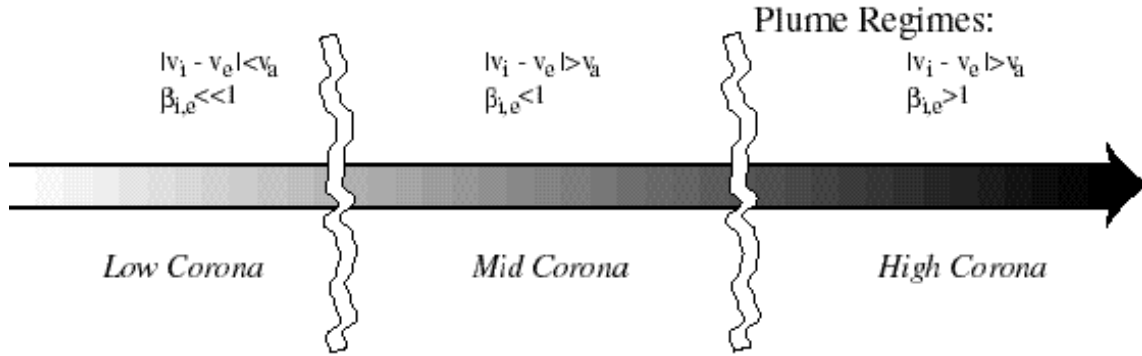


Figure 9. Different plume regimes in shear velocity ($|v_i - v_e|$) and β in the corona. v_a is the Alfvén speed. 'i' and 'e' refer to internal and external to the plume. The plume is initially subAlfvénic in a low- β plasma. For moderate shear ($> \sim 300$ km/s) it first becomes superAlfvénic and then moves into a high- β plasma.

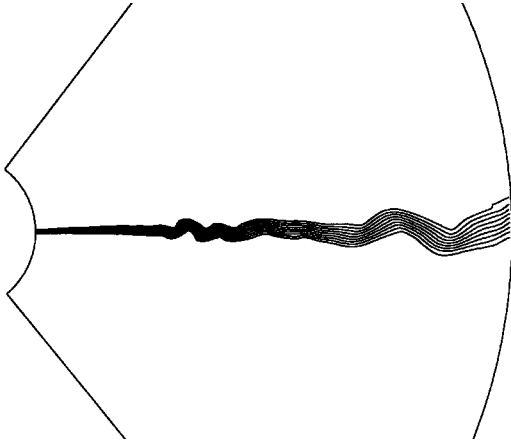


Figure 10. Magnetic field lines for a jet moving into an expanding external atmosphere in cylindrical geometry (Hardee and Clarke, 1995). The jet is magnetized and remains stable until it becomes superAlfvénic. It then destabilizes abruptly. There is no field in the external medium.

Presently, simulations are under way for conditions more appropriate for coronal plumes (Parhi & Suess, 1998; Suess et al., 1998b). These simulations use the same numerical code used by Hardee, the so-called ZEUS code. The present version is fully 3D, time dependent, and contains the metrics for calculations in Cartesian, cylindrical, or spherical coordinate systems. Preliminary simulations are being made only in Cartesian slab geometries in order to carefully map out the parameter regime.

5. SUMMARY

Plume flow can be well-simulated by applying standard 1D, time dependent solar wind models. Several appropriate models already exist, including those of Hu (1997) and Habbal et al. (1995). Plume geometry is incorporated through the use of a spreading function. The differences between plume and interplume solar wind models are in the heating and

momentum source terms and in the spreading function near the base.

The spreading function is calculated by combining a potential field calculation at the base, to account for the magnetic flux concentrations located there, with a global MHD coronal model above heights of $\sim 50,000$ km. Plume and adjacent interplume spreading functions are essentially identical between $50,000$ km and where the plasma becomes O[1] or where the plume starts mixing with the interplume. The total spreading between the base of plumes and the interplanetary medium is between 30 for large coronal holes and ~ 200 for small coronal holes. This also depends on the background magnetic field in between photospheric magnetic flux concentrations. A 5% background (in strength) is used here.

The inferred mixing of plume and interplume plasma is not a resolved process. However, such ideas as the “pulsed solar wind model” of Feldman et al. (1998) do not apply since they only address mixing along flux tubes, not across flux tubes. Plumes *will* be subject to the MHD KH instability if the shear speed is greater than the Alfvén speed. Because the ambient Alfvén speed decreases with increasing heliocentric distance, becoming generally < 50 km/s at 1 AU, almost any shear will eventually become unstable. It appears that shear associated with plumes will become unstable at $15 \pm 10 R_{\text{SUN}}$, generating Alfvénic fluctuations because the ambient $\ll 1$ and becoming a potential source for such fluctuations seen further from the Sun in the solar wind.

6. UNRESOLVED ISSUES

Although plume modeling is under way, it has not gone very far. Much more is needed. An incomplete list of useful additions is offered here:

1. Application of the best 1D models to plumes (i.e. dense, slow wind).
2. Incorporation of rapid basal spreading, shown by Del Zanna et al. (1997) to have an important effect on mass flux.
3. Parameteric survey of consequences of changing the photospheric field morphology and strength.
4. Time dependences: This category requires some comment. Many time fluctuations have been reliably reported at the base of plumes and, more anecdotally, moving up plumes. Bright points and flaring bright points sometimes lie at the base of plumes. It seems obvious that transients in plumes are an open area for modeling but nothing has been done. Since the most user-friendly plume models are inherently time dependent, much could be learned by using them to study transients.
5. Finally, plume/interplume mixing is an open area for study.

ACKNOWLEDGMENTS

Support for this research was provided by the Ulysses/SWOOPS and SOHO/UVCS projects.

REFERENCES

- Ahmad, I.A., and Withbroe, G.L. 1977, EUV analysis of polar plumes, *Sol.Phys.*, **53**, 397.
- Chandrasekhar, S. 1961, “Hydrodynamic and Hydromagnetic Stability,” Oxford University Press.
- Corti, G., Poletto, G., Romoli, M., Kohl, J., Noci, G. 1997, in “The corona and solar wind near minimum activity” (Fifth SOHO Workshop, B. Fleck ed.), ESA SP-404, p.289.
- DeForest, C.E., Hoeksema, J.T., Gurman, and five others 1998, Polar Plume Anatomy: Results of a coordinated observation, *Sol.Phys.*, **175**(2), 393-410.
- Del Zanna, L., Hood, A.W., and Longbottom, A.W. 1997, An MHD model for solar coronal plumes, *A&A*, **381**(3), 963.
- Feldman, W.C., Habbal, S.R., Hoogeveen, G., and Wang, Y-M. 1997, Experimental constraints on pulsed and steady-state models of the solar wind near the Sun, *J.Geophys.Res.*, **102**, 26,905.
- Grall, R.R., Coles, W.A., Klinglesmith, M.T., Breen, A.R., Williams, P.J.S., Markkanen, J., and Esser, R. 1996, Rapid acceleration of the polar solar wind, *Nature*, **379**, 429.
- Habbal, S.R., Esser, R., Guhathakurta, M., and Fisher, R.R. 1995, Flow properties of the solar wind derived from a two-fluid model with constraints from white light and in situ interplanetary observations, *Geophys.Res.Lett.*, **22**, 1465.
- Hardee, P.E., Cooper, M.A., Norman, M.L., and Stone, J.M. 1992, Spatial stability of the magnetized slab jet, *ApJ*, **399**, 478.
- Hardee, P.E. 1995, Unstable long wavelength magnetohydrodynamic waves on highly collimated outflows, *Ann.New York Acad.Sci.*, **773**, 14.
- Hardee, P.E., and Clarke, D.A. 1995, Destabilization of strongly magnetized jets, *ApJ*, **449**, 119.
- Hu, Y.-Q., Esser, R., and Habbal, S.R. 1997, A fast solar wind model with anisotropic proton temperature, *J.Geophys.Res.*, **102**, 14,661.
- Kopp, R.A., and Holzer, T.E. 1977, Dynamics of coronal hole regions I. Steady polytropic flows with multiple critical points, *Sol.Phys.*, **49**, 43.
- Krogulec, M., Musielak, Z.E., Suess, S.T., Nerney, S.F., and Moore, R.L. 1994, Reflection of Alfvén waves in the solar wind, *J.Geophys.Res.*, **99**, 23,489.

- McComas, D.J., Barraclough, B.L., Gosling, J.T., Hammond, C.M., Neugebauer, M., Balogh, A., and Forsyth, R.J. 1995, Structures in the polar solar wind: Plasma and field observations from Ulysses, *J.Geophys.Res.*, *100*, 19,893.
- Munro, R.H., and Jackson, B.V. 1977, Physical properties of a polar coronal hole from 2 to 5 R_{SUN} , *ApJ*, *213*, 874.
- Neugebauer, M., Goldstein, B.E., McComas, D.J., Suess, S.T., and Balogh, A. 1995, Ulysses observations of microstreams in the solar wind from coronal holes, *J.Geophys.Res.*, *100*, 23,389.
- Newkirk, G., and Harvey, J. 1968, Coronal polar plumes, *Sol.Phys.*, *3*, 321.
- Parhi, S., Suess, S.T., and Sulkanen, M. 1998, Can Kelvin-Helmholtz instabilities of jet-like structures and plumes cause solar wind fluctuations at 1 AU?, *EOS* (Spring'98 AGU) in press.
- Phillips, J.L., Bame, S.J., Barnes, A., Barraclough, B.L., Feldman, W.C., Goldstein, B.E., Gosling, J.T., Hoogeveen, G.W., McComas, D.J., Neugebauer, M., and Suess, S.T. 1995, Ulysses solar wind plasma observations from pole to pole, *Geophys.Res.Lett.*, *22*, 3301.
- Poletto, G., Corti, G., Kohl, J., Noci, G., and Suess, S.T. 1997, Expansion factors in coronal holes and plume/interplume UVCS observations, *B.A.A.S.*, *29*(2), 880.
- Rosner, R., Tucker, W.H., and Viana, G.S. 1978, Dynamics of the quiescent solar corona, *ApJ*, *220*, 643.
- Steinolfson, R.S., Suess, S.T., and Wu, S.T., The steady global corona 1982, *Ap.J.*, *255*, 730.
- Suess, S. T. 1982a, Unsteady, thermal conductive coronal flow, *ApJ*, *259*, 880.
- Suess, S.T. 1982b, Polar coronal plumes, *Sol.Phys.*, *75*, 145.
- Suess, S.T. 1988, Estimated wave speeds in coronal holes and streamers, in "Solar and Stellar Coronal Structure and Dynamics" (R. C. Altrock, ed.), p 130, National Solar Observatory/Sacramento Peak, Sunspot, New Mexico.
- Suess, S.T., Wang, A.-H., and Wu, S.T. 1996, Volumetric heating in coronal streamers, *J.Geophys.Res.*, *101*, 19,957.
- Suess, S.T., and Smith, E.J. 1996, Latitudinal dependence of the radial IMF component: coronal imprint, *Geophysy.Res.Lett.*, *23*, 3267.
- Suess, S.T., Smith, E.J., Phillips, J., Goldstein, B.E., and Nerney, S. 1996, Latitudinal dependence of the radial IMF component: interplanetary imprint, *A&A*, *316*, 304.
- Suess, S.T., Poletto, G., Wang, A.-H., Wu, S.T., and Cuseri, I. 1998a, The geometric spreading of coronal plumes and coronal holes, *Sol.Phys.* in press.
- Suess, S.T., Parhi, S., and Moore, R. 1998b, The paradox of filamented coronal hole flows but uniform high speed wind, *EOS* (Spring'98 AGU) in press.
- Velli, M., Habbal, S.R., and Esser, R. 1994, Coronal plumes and the fine scale structure in high speed solar wind streams, *Spa.Sci.Rev.*, *70*, 391.
- Wang, A.-H., Wu, S.T., Suess, S.T., and Poletto, G. 1998, Global model of the corona with heat and momentum addition, *J.Geophys.Res.*, *103*, 1913.
- Wang, Y.-M. 1994, Polar plumes and the solar wind, *Ap.J. Lett.*, *435*, L153.